ChemComm

COMMUNICATION

Luminescent mechanochromism of a chiral complex: Distinct crystal structure and color changes of racemic and homochiral gold(I) isocyanide complexes with a binaphthyl moiety

Received 00th January 20xx,
Accepted 00th January 20xx

DOI: 10.1039/x0xx00000x

www.rsc.org/

Mingoo Jin,[a] Tomohiro Seki[a*] and Hajime Ito[a*]

Luminescent mechanochromism of a chiral gold(I) complex is investigated. The racemic and homochiral forms of the gold(I) complex possess distinct crystal packing arrangements with different emission colors. Upon mechanical stimulation, both crystals transform into amorphous powders that exhibit similar emission colors.

Mechanochromic luminescent compounds based on organic and organometallic compounds have recently attracted attention because of potential applications in sensing and recording devices.[1] The luminescence properties of many mechanochromic compounds are strongly correlated with their molecular packing arrangements in the solid state.[2] Therefore, controlling the molecular arrangements of mechanochromic compounds is important to tune their emission properties.

Racemic and homochiral compounds often crystallize into different structures that show different physical properties even though they have the same chemical composition. Wallach's rule states that racemic crystals tend to be denser than their homochiral equivalents.[3] Based on this viewpoint, crystals of racemic and homochiral compounds have been investigated with the aim of controlling the molecular packing arrangement in the solid phase and the resulting physical properties.[4]

In 1982, Roitman *et al.*[5a] reported that racemic and homochiral 1-phenylpropyl 9-anthroate crystals display obviously different emission properties. Numerous crystals with different enantiomer compositions that afford distinct emission properties have been reported.[5] However, the different mechanochromic properties of racemic and homochiral crystalline luminescent materials have not been investigated.[6]

We previously reported reversible luminescent mechanochromism of [$(C_6F_5Au)_2$(μ-1,4-)]diisocyanobenzene.[2a] Based on this finding, we successfully developed several mechanochromic compounds that display various mechanoresponsive emission color changes. Introducing triethylene glycol side chains into the above aryl gold(I) isocyanide complex resulted in novel mechanochromism based on crystal-to-crystal transformation mediated by a transient amorphous state.[7a] A similar compound bearing 4-perfluoropyridyl gold(I) moieties instead of pentafluorophenyl gold(I) exhibits four different emission colors that are interconvertible through mechanical stimulation and solvent exposure.[7b] Recently, we reported complexes showing mechano-induced single-crystal-to-single-crystal phase transitions.[7c,d]

Through these studies, we realized that the aryl gold(I) isocyanide moiety is an excellent basic structure to produce new mechanochromic materials. We anticipate that aryl gold(I) isocyanides could be modified with chiral structures to afford new mechanochromic complexes. Herein, we report binaphthyl gold(I) isocyanide complex **1**, which possesses an axially chiral moiety. Crystals prepared from racemic [(*rac*)-**1**] and homochiral [(*S*)-**1**] complexes display distinct emission colors. These two different crystals exhibit luminescent mechanochromism, showing similar red-shifted emission after grinding (Fig. 1a and b). This is the first comparison of mechanochromism in racemic and homochiral crystals of a chiral compound.

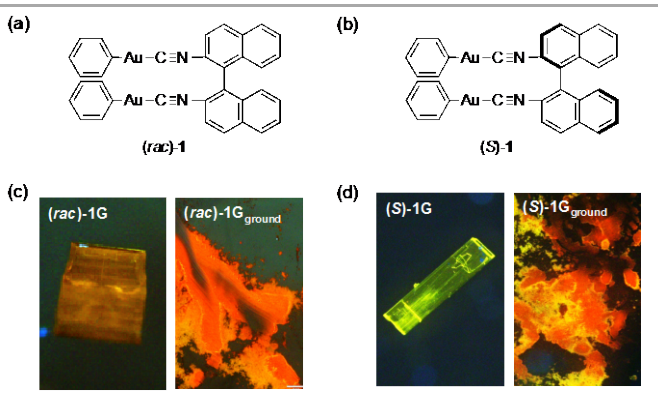

Fig. 1 Structure of (a) (*rac*)-**1** and (b) (*S*)-**1**. Photographs of (c) (*rac*)-**1G** and (*rac*)-**1G**$_{ground}$ and (d) (*S*)-**1G** and (*S*)-**1G**$_{ground}$ taken under ultraviolet irradiation (λ_{ex} = 365 nm).

[a] *Division of Applied Chemistry and Frontier Chemistry Center, Faculty of Engineering, Hokkaido University, Sapporo, Hokkaido 060-8628, Japan. E-mail: hajito@eng.hokudai.ac.jp*

†Electronic Supplementary Information (ESI) available: X-ray crystallographic data, optical properties, TGA profiles, and other additional information. CCDC 1472283 and 1472333. For ESI and crystallographic data in CIF or other electronic format see DOI: 10.1039/c000000x/

Gold(I) isocyanide complexes (*rac*)-**1** and (*S*)-**1** were synthesized from the corresponding chiral isocyanide gold(I) complex precursors, (*rac*)-2,2'-[NC-Au(I)-Cl]$_2$-binaphthyl and (*S*)-2,2'-[NC-Au(I)-Cl]$_2$-binaphthyl, respectively,[8] through modification of our reported procedures.[7] Crystallization of (*rac*)-**1** from CH_2Cl_2/hexane for 6 h afforded cubic crystals of (*rac*)-**1G** that displayed yellowish green emission under ultraviolet irradiation (Fig. 1c, λ_{ex} = 365 nm). The same crystallization process of (*S*)-**1** afforded hexahedral crystals of (*S*)-**1G** showing green emission (Fig. 1d), which is clearly different from that of (*rac*)-**1G** crystals. Both (*rac*)-**1G** and (*S*)-**1G** displayed luminescent mechanochromism (Fig. 1c and d). When the yellowish green-emitting crystals of (*rac*)-**1G** were ground by a mortar and pestle or ball mill at room temperature, a powder of (*rac*)-**1G$_{ground}$** exhibiting red emission was formed. Similar mechanical stimulation of the green-emitting crystals of (*S*)-**1G** gave the powder (*S*)-**1G$_{ground}$**, which has a similar emission color to that of (*rac*)-**1G** crystals.

To investigate the structure of each phase, single-crystal X-ray diffraction (XRD) analyses of (*rac*)-**1G** and (*S*)-**1G** crystals as well as powder XRD analyses of the ground samples (*rac*)-**1G$_{ground}$** and (*S*)-**1G$_{ground}$** were performed. Single-crystal XRD analysis revealed that (*rac*)-**1G** crystallized in the *Pbcn* space group. In the (*rac*)-**1G** crystal, two molecules of the same enantiomer formed a dimer unit, denoted as an *S*-*S* or *R*-*R* dimer, where each molecule was connected through aurophilic interactions with Au–Au distances of 3.06, 3.34, and 3.06 Å and CH–π interactions (Fig. 2a). Both the *S*-*S* and *R*-*R* dimers contained an inversion center (red dots in Fig. 2b and c). The *S*-*S* dimers adopted a layer structure, denoted as an *S*-type layer. Adjacent to the *S*-type layer, an *R*-type layer formed through the interactions of *R*-*R* dimers (Fig. 2c). The crystalline lattice contained CH_2Cl_2, which was used for recrystallization.

The crystal structure of (*S*)-**1G** was quite different from that of (*rac*)-**1G**. (*S*)-**1G** crystallized in the chiral space group $P2_12_12_1$. In the crystal, two (*S*)-**1** molecules formed a dimer unit, similar to those found in (*rac*)-**1G**. Each dimer was held together by three aurophilic bonds with Au–Au distances of 3.07, 3.14, and 3.16 Å and CH– π interactions (Fig. 2d). The relative arrangement of dimers in (*S*)-**1G** was markedly different from that in (*rac*)-**1G**. In the case of (*S*)-**1G**, two adjacent *S*-*S* dimers were packed as shown in Fig. 2e and S11 and there were no inversion centers. This difference of dimer arrangement reflects how the layer structure of (*S*)-**1G** is distinct from that of (*rac*)-**1G** (Fig. 2c and f). Disordered CH_2Cl_2 molecules were located between the two adjacent dimers (Fig. 2f).

The structural changes of (*rac*)-**1G** and (*S*)-**1G** induced by mechanical stimulation were observed by powder XRD measurements. Ground powders (*rac*)-**1G$_{ground}$** and (*S*)-**1G$_{ground}$** were prepared by ball milling (*rac*)-**1G** and (*S*)-**1G** for 30 min at 4600 rpm, respectively. The lack of features in the powder XRD patterns of (*rac*)-**1G$_{ground}$** and (*S*)-**1G$_{ground}$** reveals that both powders are amorphous (orange lines in Fig. 3a and b). As already mentioned above, crystals of (*rac*)-**1G** and (*S*)-**1G** included 0.25 and 0.5 equiv. of CH_2Cl_2 molecules in each crystalline lattice, respectively [thermogravimetric analysis (TGA) (Fig. S1), ^{1}H NMR spectral data (Fig. S2), and single-crystal XRD analysis (Fig. S3 and S4) are presented in ESI]. In contrast, elemental analyses, TGA and ^{1}H NMR spectroscopy of (*rac*)-**1G$_{ground}$** and (*S*)-**1G$_{ground}$** revealed that both the ground powders do not include CH_2Cl_2 molecules (Table S1, Fig. S1 and S2). The CH_2Cl_2 molecules in both (*rac*)-**1G** and (*S*)-**1G** can be removed by holding the samples under vacuum at 65 °C for 1 h (Fig S5). Both (*rac*)-**1G** and (*S*)-**1G** remained crystalline after removal of CH_2Cl_2, and their emission colors did not change (Fig. S6–S8).

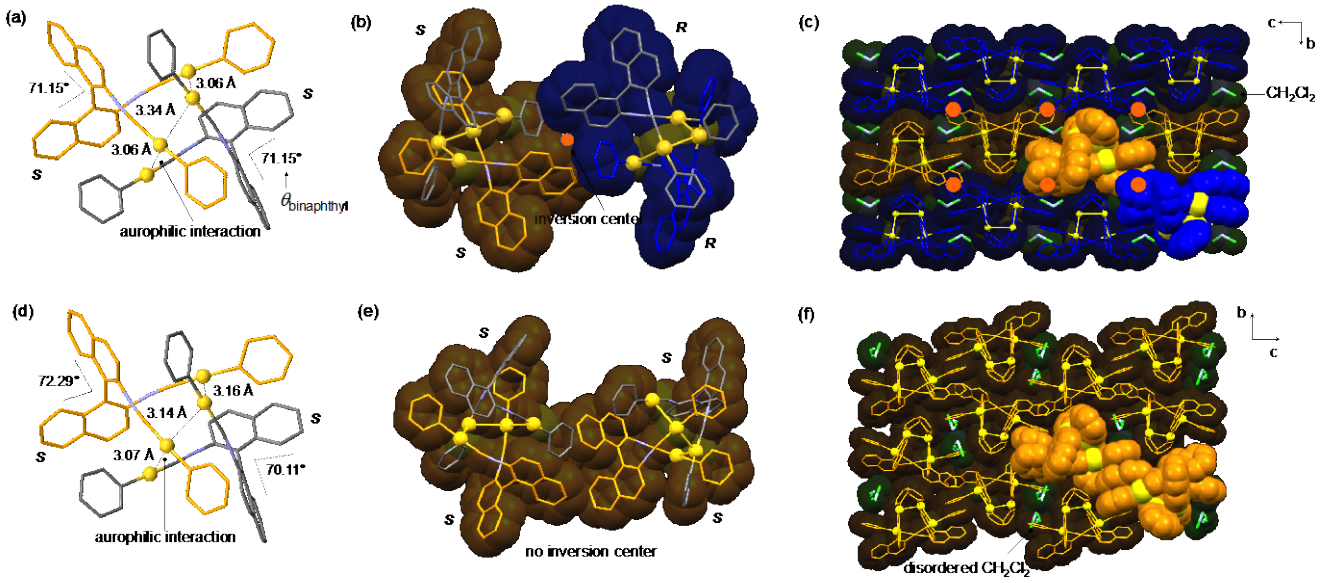

Fig. 2 Single-crystal structures of (a–c) (*rac*)-**1G**, and (d–f) (*S*)-**1G**. (a) Dimer, (b) tetramer, and (c) layer structures of (*rac*)-**1G**. (d) Dimer, (b) tetramer, and (c) layer structures of (*S*)-**1G**. All H atoms were omitted for clarity.

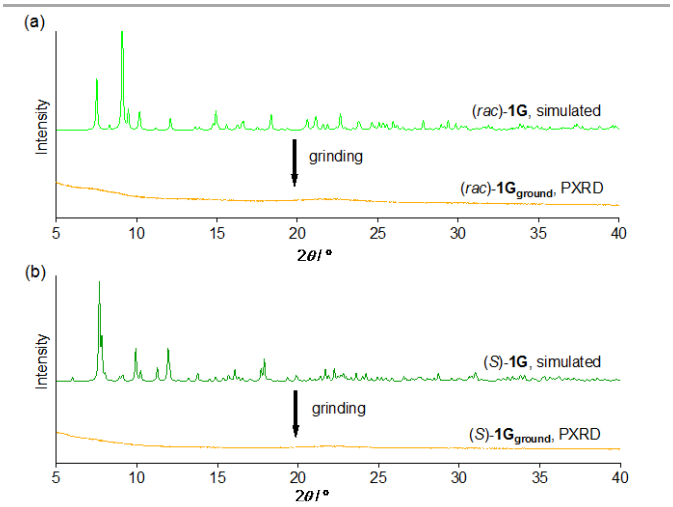

Fig. 3 PXRD pattern changes from (a) (*rac*)-**1G** (light green line, simulated pattern) to (*rac*)-**1G**$_{\mathbf{ground}}$ (orange line) and (b) (*S*)-**1G** (green line, simulated pattern) to (*S*)-**1G**$_{\mathbf{ground}}$ (orange line).

Emission spectroscopy measurements of pristine (*rac*)-**1G** and (*S*)-**1G** and their ground phases were performed. The emission spectrum of (*rac*)-**1G** is broad with a maximum emission wavelength $\lambda_{em,max}$ of 546 nm upon excitation at 365 nm (light green solid line in Fig. 4a). Upon grinding, the emission of (*rac*)-**1G** shows a clear red shift. The ground powder (*rac*)-**1G**$_{\mathbf{ground}}$ exhibited a broad emission spectrum with $\lambda_{em,max}$ at 664 nm (orange solid line in Fig. 4a). The emission spectrum of (*S*)-**1G** (green solid line in Fig. 4a) is different from that of (*rac*)-**1G**. For example, $\lambda_{em,max}$ of (*S*)-**1G** is 517 nm, which is shorter than that of (*rac*)-**1G**. In contrast, the emission spectrum of (*S*)-**1G**$_{\mathbf{ground}}$ ($\lambda_{em,max}$ = 664 nm, red solid line in Fig. 4a) is almost the same as that of (*rac*)-**1G**$_{\mathbf{ground}}$.

Excitation spectra of the samples were measured. The excitation spectrum of (*rac*)-**1G** contained a broad band ranging from 350 to 480 nm with a maximum excitation wavelength $\lambda_{ex,max}$ of 454 nm (λ_{em} = 546 nm, light green solid line in Fig. 4b). The excitation spectrum of (*rac*)-**1G**$_{\mathbf{ground}}$ also possessed a similar broad band with $\lambda_{ex,max}$ = 449 nm (λ_{em} = 546 nm, orange solid line in Fig. 4b). In the case of (*S*)-**1G**, similar excitation spectral changes were observed. The excitation spectrum of (*S*)-**1G** obtained at 517 nm contained a broad band spanning 350–500 nm with $\lambda_{ex,max}$ = 458 nm (green solid line in Fig. 4b). In the case of (*S*)-**1G**$_{\mathbf{ground}}$, a similar broad excitation spectrum with $\lambda_{ex,max}$ = 445 nm was observed at 664 nm. This result indicates that the excitation spectra of this system are not strongly influenced by distinct molecular packing arrangements.

Emission lifetimes and quantum yields Φ_{em} of both crystals and their ground powders were measured. (*rac*)-**1G** showed a low Φ_{em} of 0.08 with an average emission lifetime τ_{av} of 5.34 μs, while the ground powder (*rac*)-**1G**$_{\mathbf{ground}}$ displayed an increased Φ_{em} of 0.21. τ_{av} of (*rac*)-**1G**$_{\mathbf{ground}}$ is 5.10 μs, which is slightly shorter than that of (*rac*)-**1G** (Table 1, Fig. S9). In the case of (*S*)-**1G**, Φ_{em} was also low (0.02). After grinding, Φ_{em} of (*S*)-**1G**$_{\mathbf{ground}}$ increased to 0.13. Meanwhile, τ_{av} of (*S*)-**1G** and (*S*)-**1G**$_{\mathbf{ground}}$ were almost the same at 5.34 and 5.36 μs, respectively (Table 1, Fig. S9). The photoluminescent intensities of (*rac*)-**1** and (*S*)-**1** in CH_2Cl_2 were very weak, so we could not measure their emission properties (Fig. S10 and S11). This indicates that the high emission intensities of solid-state (*rac*)-**1** and (*S*)-**1** strongly depend on their aggregated structures.[9]

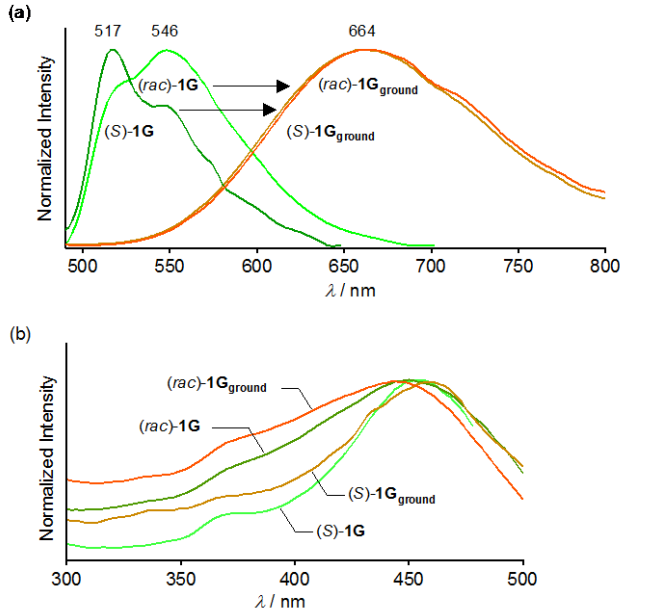

Fig. 4 (a) Emission spectra changes from (*rac*)-**1G** to (*rac*)-**1G**$_{\mathbf{ground}}$, and from (*S*)-**1G** to (*S*)-**1G**$_{\mathbf{ground}}$ (λ_{ex}=365 nm). (b) Excitation spectra of (*rac*)-**1G**, (*S*)-**1G**, (*rac*)-**1G**$_{\mathbf{ground}}$, and (*rac*)-**1G**$_{\mathbf{ground}}$ obtained at each $\lambda_{em,max}$.

Table 1 Photophysical properties of (*rac*)-**1G**, (*S*)-**1G**, (*rac*)-**1G**$_{\mathbf{ground}}$, and (*S*)-**1G**$_{\mathbf{ground}}$

	$\lambda_{em,max}$ [a] / nm	Φ_{em} (λ_{ex} / nm) / %	τ_{av} [b] (λ_{em} / nm)/ μs
(*rac*)-**1G**	546	0.08 (454)	5.34 (546)
(*S*)-**1G**	517	0.02 (458)	5.34 (517)
(*rac*)-**1G**$_{\mathbf{ground}}$	664	0.21 (449)	5.10 (664)
(*S*)-**1G**$_{\mathbf{ground}}$	664	0.13 (445)	5.36 (664)

[a]: maximum emission wavelength (λ_{ex} = 365 nm), [b]: $\tau_{av} = \Sigma \tau_n A_n^2 / \Sigma \tau_n A_n$, obtained by tail fitting (λ_{ex} = 370 nm).

The relationships between the emission properties and crystal structures of each phase are now discussed. Dimer units constructed from two molecules of the same enantiomer, such as *S*-*S* dimers, are observed in both (*rac*)-**1G** and (*S*)-**1G**. The fundamental structures of dimers found in (*rac*)-**1G** and (*S*)-**1G** crystals are very similar. For example, three aurophilic bonds are present in both crystals, and the average Au–Au distances of (*rac*)-**1G** and (*S*)-**1G** are 3.15 and 3.12 Å, respectively, which is a difference of only 0.03 Å. The minimum dihedral angle between the naphthyl groups of the binaphthyl moiety ($\theta_{binaphthyl}$) of (*rac*)-**1G** was 71.15°, and that of (*S*)-**1G** was 70.11°. The average $\theta_{binaphthyl}$ of dimers in (*rac*)-**1G** and (*S*)-**1G** were 71.15° and 71.20°, respectively (Fig. 2a and 2d). Therefore, the considerable structural difference between crystalline (*rac*)-**1G** and (*S*)-**1G** probably lies in the relative arrangements of the dimer units rather than the structure of the dimer unit itself. The powder XRD patterns suggest that both (*rac*)-**1G**$_{\mathbf{ground}}$ and (*S*)-**1G**$_{\mathbf{ground}}$ adopt random molecular arrangements, indicating collapse of the dimer packing upon mechanical stimulation (Fig. 5). Both ground powders show similar

red-shifted emission with higher Φ_{em} than those of their parent crystals. Because a red shift of emission and increase of Φ_{em} are typically observed for mechanochromic gold(I) isocyanide complexes, these experimental results suggest that the aurophilic interactions strengthen after mechanical stimulation.[7] The elaborated crystal structure and photophysical property differences between (*rac*)-**1** and (*S*)-**1** crystals, which originated from different enantiomer compositions, were amalgamated into uniform amorphous structures with similar emission colors by grinding. It should be noted that only mechanical stimulation promoted this amorphization with the disappearance of the individuality of racemic and homochiral crystals.

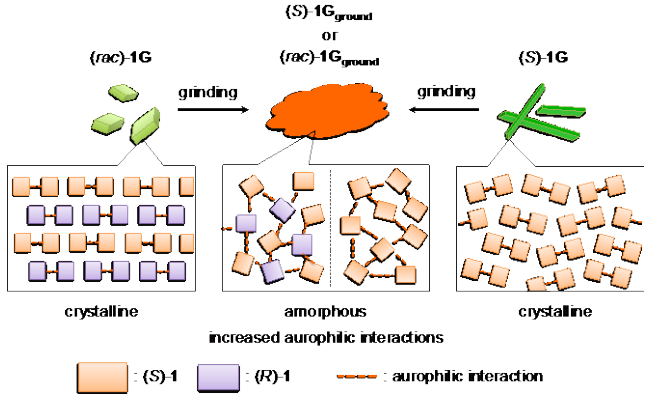

Fig. 5 Top: schematics of mechanochromism of (*rac*)-**1G** converting to (*rac*)-**1G** $_{ground}$ (from left to center) and (*S*)-**1G** converting to (*S*)-**1G** $_{ground}$ (from right to center). Bottom: schematics of the corresponding molecular arrangements in which orange and purple rectangles represent (*S*)-**1** and (*R*)-**1** molecules, respectively.

Racemic and homochiral forms of gold(I) isocyanide complex **1** possessing a binaphthyl moiety with distinct luminescent crystals that exhibit mechanochromism. Crystals of (*rac*)-**1G** and (*S*)-**1G** showed distinct emission colors and different crystal packing structures. The powders obtained by grinding both crystals were amorphous and displayed similar emission colors. This is the first example of luminescent mechanochromism of racemic and homochiral compounds that display distinct emission colors. These results indicate that the introduction of chirality can be a promising structure modification to tune the properties of mechanochromic materials.

Notes and references

This work was financially supported by the Ministry of Education, Culture, Sports, Science and Technology (Japan) program "Strategic Molecular and Materials Chemistry through Innovative Coupling Reactions" of Hokkaido University; Building of Consortia for the Development of Human Resources in Science and Technology, "Program for Fostering Researchers for the Next Generation"; The Ministry of Education, Culture, Sports, Science and Technology through a Program for Leading Graduate Schools, Hokkaido University "Ambitious Leader's Program"; and by Japan Society for the Promotion of Science KAKENHI (Grant Nos. 15H03804, 15K13633, and 16H06034). We also thank the Frontier Chemistry Center Akira Suzuki "Laboratories for Future Creation" Project, Hokkaido University.

1 (a) Z. Chi, X. Zhang, B. Xu, X. Zhou, C. Ma, Y. Zhang, S. Liu and J. Xu, *Chem. Soc. Rev.*, 2012, **41**, 3878–3896; (b) X. Zhang, Z. Chi, Y. Zhang, S. Liu and J. Xu, *J. Mater. Chem. C*, 2013, **1**, 3376–3390; (c) Y. Sagara and T. Kato, *Nat. Chem.*, 2009, **1**, 605–610; (d) A. L. Balch, *Angew. Chem. Int. Ed.*, 2009, **48**, 2641–2644; (e) C. Jobbágy and A. Deák, *Eur. J. Inorg. Chem.*, 2014, **2014**, 4434–4449. (f) Y. Sagara, S. Yamane, M. Mitani, C. Weder and T. Kato, *Adv. Mater.*, 2016, **28**, 977–1326.

2 (a) H. Ito, T. Saito, N. Oshima, N. Kitamura, S. Ishizaka, Y. Hinatsu, M. Wakeshima, M. Kato, K. Tsuge and M. Sawamura, *J. Am. Chem. Soc.*, 2008, **130**, 10044–10045; (b) M. Osawa, I. Kawata, S. Igawa, M. Hoshino, T. Fukunaga and D. Hashizume, *Chem. Eur. J.*, 2010, **16**, 12114–12126; (c) S. Varughese, *J. Mater. Chem. C*, 2014, **2**, 3499–3516; (d) Y. Hong, J. W. Lam and B. Z. Tang, *Chem. Soc. Rev.*, 2011, **40**, 5361–5388; (e) M. Shimizu and T. Hiyama, *Chem. Asi. J.*, 2010, **5**, 1516–1531; (f) J. Gierschner and S. Y. Park, *J. Mater. Chem. C*, 2013, **1**, 5818–5832; (g) Y. Sagara, T. Mutai, I. Yoshikawa and K. Araki, *J. Am. Chem. Soc.*, 2007, **129**, 1520–1521; (h) G. Zhang, J. Lu, M. Sabat and C. L. Fraser, *J. Am. Chem. Soc.*, 2010, **132**, 2160–2162.

3 (a) O. Wallach, *Liebigs Ann. Chem.*, 1895, **286**, 90-143; (b) C. P. Brock, W. B. Schweizer and J. D. Dunitz, *J. Am. Chem. Soc.*, 1991, **113**, 9811–9820.

4 (a) K. J. Stine, J. Y. J. Uang and S. D. Dingman, *Langmuir*, 1993, **9**, 2112–2118; (b) L. Brammer, *Chem. Soc. Rev.*, 2004, **33**, 476–489; (c) J. Zhang, Y. G. Yao and X. Bu, *Chem. Mater.*, 2007, **19**, 5083–5089; (d) A. J. Bailey, C. Lee, R. K. Feller, J. B. Orton, C. Mellot-Draznieks, B. Slater, W. T. A. Harrison, P. Simoncic, A. Navrotsky, M. C. Grossel and A. K. Cheetham, *Angew. Chem. Int. Ed.*, 2008, **47**, 8634–8637.

5 (a) Z. Ludmer, M. Lahav, L. Leiserowitz and L. Roitman, *J. Chem. Soc., Chem. Commun.*, 1982, **6**, 326–328; (b) C. D. Delfs, H. J. Kitto, R. Stranger, G. F. Swiegers, S. B. Wild, A. C. Willis and G. J. Wilson, *Inorg. Chem.*, 2003, **42**, 4469–4478; (c) E. C. Yang, H. K. Zhao, B. Ding, X. G. Wang and X. J. Zhao, *Crystal Growth & Design*, 2007, **7**, 2009–2015; (d) K. A. McGee and K. R. Mann, *J. Am. Chem. Soc.*, 2009, **131**, 1896–1902; (e) T. F. Mastropietro, Y. J. Yadav, E. I. Szerb, A. M. Talarico, M. Ghedini and A. Crispini, *Dalton Trans.*, 2012, **41**, 8899–8907.

6 For chiral Pt(II) complexes: the two enantiomers of Pt(II) complexes show chiroptical property switching upon mechanical stimulation; X. P. Zhang, J. F. Mei, J. C. Lai, C. H. Li and X. Z. You, *J. Mater. Chem. C*, 2015, **3**, 2350–2357.

7 (a) S. Yagai, T. Seki, H. Aonuma, K. Kawaguchi, T. Karatsu, T. Okura, A. Sakon, H. Uekusa and H. Ito, *Chem. Mater.*, 2016, **28**, 234–241; (b) T. Seki, T. Ozaki, T. Okura, K. Asakura, A. Sakon, H. Uekusa and H. Ito, *Chem. Sci.*, 2015, **6**, 2187–2195; (c) H. Ito, M. Muromoto, S. Kurenuma, S. Ishizaka, N. Kitamura, H. Sato and T. Seki, *Nat. Commun.*, 2013, **4**, 2009; (d) T. Seki, K. Sakurada and H. Ito, *Angew. Chem. Int. Ed.*, 2013, **52**, 12828–12832.

8 C. Bartolome, D. Garcia-Cuadrado, Z. Ramiro and P. Espinet, *Inorg. Chem.*, 2010, **49**, 9758–9764.

9 (a) Y. Hong, J. W. Y. Lam and B. Z. Tang, *Chem. Soc. Rev.*, 2011, **40**, 5361–5388. (b) N. B. Shustova, B. D. McCarthy and M. Dinca, *J. Am. Chem. Soc.*, 2011, **133**, 20126–20129.